Chemical Physics Letters 503 (2011) 112–117

Contents lists available at ScienceDirect

Chemical Physics Letters

journal homepage: www.elsevier.com/locate/cplett

Molecular dynamics simulation of energetic aluminum/palladium core–shell nanoparticles

Ngoc Ha Nguyen [a,b], Anming Hu [a], John Persic [c], John Z. Wen [a,*]

[a] University of Waterloo, Department of Mechanical and Mechatronics Engineering, Waterloo, ON, Canada N2L 3G1
[b] Hanoi National University of Education, Department of Chemistry, Center for Computational Science, Hanoi, VietNam
[c] Microbonds Inc., 151 Amber St., Unit 12 Markham, ON, Canada L3R 3B3

ARTICLE INFO

Article history:
Received 18 November 2010
In final form 23 December 2010
Available online 27 December 2010

ABSTRACT

This Letter presents the thermal stability and energetic reaction properties of palladium coated aluminum nanoparticles. The classical MD simulations are conducted using a new EAM force field. The results reveal that, when the initial temperature is higher than 600 K and lower than 900 K, a two-stage reaction may occur. At the first stage, the reaction rate is determined by the solid-state diffusion of Al atoms. At the second stage where the particle temperature is greater than the melting point of Al, the alloying reaction between the liquid Al core and the Pd shell happens with a much faster rate.

1. Introduction

Nanostructured energetic materials have shown promising applications in powering microelectromechanical systems (MEMS) and developing advanced material joining techniques [1]. Passivated aluminum nanoparticles, as a major component of metastable intermolecular composites or MICs, have been most extensively investigated for formulating nanopropellants and nanothermites with superior ignition and reaction properties [2]. The performance of these composites such as reaction rates and ignition temperatures depends greatly on the degree of mixing of the oxidizer (e.g., CuO, Fe_2O_3, and other oxide nanoparticles) and the reducing agent (i.e., Al nanoparticles). A number of experimental studies have been recently conducted to improve the interfacial contact between the oxide and Al components [3–8]. Meanwhile, the development of bimetallic nanothermites, especially composed of an Al core and a metallic shell, has drawn increasing attentions in producing the high-efficiency energetic nanomaterial [9–14]. In contrary to the MIC, these core–shell nanoparticles provide a direct interface between two reactive components and hence facilitate the thermite reaction. This structural characteristic is very important for both MEMS and micro-joining applications where the precisely controlled manufacturing processes are required. The energy release data (per unit volume of reactants) for a variety of Al based bimetallic reactions, in comparison with the MICs, can be found in literature [15]. It showed clearly, although most bimetallic thermite reactions produce considerably less energy than the MICs, the bimetallic reaction between Al and Pd components can generate a comparable energy level (2890 cal/cm^3) with the MICs (3947 cal/cm^3 for Al/Fe_2O_3). In addition, since the core–shell nanothermites often exhibit lower ignition temperatures than the composites [3], the binary Al/Pd core–shell nanoparticles become an important candidate in powering MEMS and achieving effective micro-joining.

When experimental investigations on energetic properties of the Al–Pd nanothermite are needed, Molecular Dynamics (MD) simulation becomes a powerful tool in designing its structure and predicting its performance. The MD studies have been conducted in predicting the thermal response of a variety of combustible core–shell nanostructures [11–14, 16–18]. Nevertheless, most of these studies focused on the Al–Ni binary nanostructure and few can be found for the Al–Pd nanoparticle. One of challenging tasks is to obtain a suitable potential field for the Al–Pd binary system. Fortunately there are a few studies which addressed the bulk structures of Al and Pd alloys with multiple components. For example, Zijlstra et al. calculated the geometrical properties of Al–Pd–Mn quasicrystals by means of an *ab initio* approach [19]. Kuruvilla et al. experimentally studied the lattice expansion of Cu–Al–Pd alloys [20]. Zhang et al. investigated the formation of decagonal quasicrystals in Al–Pd–Ru alloys [21]. It is worthwhile to highlight an earlier work done by Koster et al. [22] who measured the bulk phases of AlPd, Al_2Pd, Al_3Pd, Al_4Pd, $AlPd_2$ and Al_3Pd_5 alloys. In that work, the transmission electron microscopy, X-ray diffraction and Auger depth profiling technique were utilized to characterize the microstructure. The obtained bulk parameters were late used by Rodbell et al. [23]. The aforementioned investigations on the geometries and properties of bulk-phase Al–Pd alloys provide a platform for developing the force field of the Al–Pd system, which is urgently needed for performing MD simulations. The major objective of this study was to reveal phase change processes and the

* Corresponding author. Fax: +1 519 885 5862.
E-mail address: jzwen@uwaterloo.ca (J.Z. Wen).

0009-2614/$ - see front matter Crown Copyright © 2010 Published by Elsevier B.V. All rights reserved.
doi:10.1016/j.cplett.2010.12.074

energetic behaviors of Pd coated Al nanoparticles. The classic MD simulations were carried out on basis of a new force field model which was developed from the literature structures and properties of bulk-phase alloys. The investigations were focused on the thermal stability and reaction properties (i.e., adiabatic combustion temperatures, reaction mechanisms and binary diffusion phenomena) of the core–shell nanoparticle.

2. Molecular dynamics simulation

A classic molecular dynamics approach was used in this study. Since the principle of the classic MD method is well known, only the critical parameters are presented here. The development of the new force field for the Al–Pd binary system is introduced first.

2.1. Force field model

For MD simulations of transition metals, the commonly used potential models include the embedded atom method (EAM) [24] and the second moment approximation for tight-binding (TB-SMA) [25,26]. Generally speaking, there is no fundamental distinction between these two models and the TB-SMA model is simpler in formulating. Mathematically for the elemental analysis, the TB-SMA potential is equivalent to an EAM potential having a square root embedding function [26]. These TB-SMA potentials used in the literature, usually developed by curve-fitting into the lattice properties of bulk crystalline phases, have been shown with good performances in predicting the characteristics of surfaces and nanosized clusters [27,28]. In this study, we implemented a similar approach by curve-fitting the TB-SMA models reported for pure Al and Pd metals [26] when the force field of the Al–Pd binary system was developed. In those TB-SMA models the potential function (or the total cohesive energy) E_C^i at the atomic site i is written as

$$E_C^i = -\left(E_R^i + E_B^i\right) \tag{1}$$

where E_R^i is the repulsive energy term and E_B^i is the band energy term. These two terms are expressed by

$$E_R^i = \sum_j A \times \exp\left[-p\left(\frac{r_{ij}}{r_0} - 1\right)\right] \tag{2}$$

$$E_B^i = -\left\{\sum_j \xi^2 \times \exp\left[-2q\left(\frac{r_{ij}}{r_0} - 1\right)\right]\right\}^{1/2} \tag{3}$$

where r_{ij} represents the distance between atoms i and j; r_0 is the inter-atomic distance between the nearest neighboring atoms; A, ζ, p and q are free model parameters and their values can be found in literature [26].

To run MD simulations, the above TB-SMA parameters were converted into the EAM density of atomic sites and the Buckingham repulsive energy components, for both pure Al and Pd metals,

$$\rho_i = A \cdot r_{ij}^n \exp(-B(r_{ij} - r_0)) \tag{4}$$

$$V_{ij} = M \cdot \exp\left(\frac{-r_{ij}}{N}\right) - \frac{C}{r_{ij}^6} \tag{5}$$

where ρ_i is the density of the atomic site i in pure metals with n, A and B as EAM fitting parameters, V_{ij} is the short-range repulsive component between i and j in the Buckingham form, and M, N and C are fitting parameters. In this study, these fitting parameters were derived from the reported TB-SMA potentials [26] and by using the fitting function of the MD code GULP [29]. Note that in order to describe the force field of the Al–Pd binary system, the scaling factors (s_i) are needed for both Al and Pd atoms. And a new set of M, N and C values should be obtained for describing the repulsive Al–Pd interactions. These five parameters were calculated using the fitting function of the GULP code and validated against the properties of the bulk Al–Pd alloy including the bulk modulus, lattice parameters and vibrations. The scaling factor is defined as

$$\rho_i' = s_i \cdot \rho_i \tag{6}$$

where ρ_i' is the density of the atomic site i in the Al–Pd alloy. Table 1 shows the derived EAM and Buckingham potential parameters in this study.

The potential data shown in Table 1 were examined by comparing the predicted bulk Al, Pd and Al–Pd properties (i.e., the lattice constant, bulk modulus and lattice vibrations) with the previously reported data. Table 2 summarizes the comparison among the computed bulk properties using the new force field and the experimental and theoretical date reported in the literature [30–32]. A good agreement was observed.

2.2. Simulation method

Initially one Al/Pd core–shell particle consisted of 2243 Al atoms and 2265 Pd atoms was constructed. Both Al and Pd atoms were arranged at 0 K with their fcc phases and the diameter of this nanoparticle was 5 nm, as shown in Figure 3a. Because it is nearly impossible to create a completely symmetrical structure for the above system, the nanoparticle has a thinner upper layer (zone **a** with less than two monolayers of Pd atoms) and a thicker bottom layer (zone **b** with two or three monolayers of Pd atoms). MD simulations were then carried out for each initial temperature (ranged from 300 K to 900 K) and through the following two-stage procedure. The time step was set to 1 fs for all simulation cases.

Step 1: Molecular dynamics relaxation. This step simulates the nanoparticle structure at the initial temperature after a specified buffer period (1 ps). At this step, the MD simulations were conducted under the canonical ensemble molecular dynamics (NVT) conditions. Totally six initial temperatures (i.e., 300 K, 400 K, 500 K, 600 K, 700 K and 900 K) were examined. It was found that after this step, the nanoparticle diameter (calculated by assuming a perfect sphere) was relaxed slightly, for example, from 5 nm to 5.16 nm at the initial temperature of 600 K. Note that the defects might exist along the interface of the Al core and the Pd shell. After this step, the original fcc phases of Al and Pd atoms were modified close to this interface, as shown later in Figure 3a.

Step 2: Molecular dynamics production. This step simulates the structural changes and energetic properties of the system under thermite reaction conditions. The computing time was set to 300 ps and the microcanonical ensemble (NVE) simulations were conducted. There was no periodic boundary conditions applied and an isolated nanoparticle system was simulated. During this step and if the thermite reaction is ignited, the energy release from the reaction will directly heat up the nanoparticle and result in its phase change. This second step of the simulation visualizes the entire process from the initiation structure to the formation of the alloyed structure by the thermite reaction. The energy release was derived from the MD simulation and the diffusion processes of Al and Pd atoms during the reaction were investigated.

Table 1
EAM and Buckingham potential parameters used in this study.

	n	A	B	r_0 [26]	s_i	M	N	C
Al	0	1.732	1.757	2.864	0.885	1342.424	0.3325	0
Pd	0	2.951	2.723	2.749	0.929	18 304.268	0.2529	0
Al–Pd						9612.573	0.2598	0

Table 2
Comparison of the model predicted bulk properties with literature values. Units: Lattice parameter a_0 (in Å), bulk modulus B (in GPa) and lattice vibrations ν (in cm^{-1}). The properties of the Al–Pd alloy were calculated in its B2 phase and with a point group of Pm3m.

	a_0			B			ν (for Al–Pd)		
	Al	Pd	Al–Pd	Al	Pd	Al–Pd	ν_4	ν_5	ν_6
Present work	4.048	3.887	3.053	81	196	159.416	274.3	274.3	274.3
Literature values	4.049 [30]	3.890 [30]	3.049 [31]	76 [32]	182 [32]	159.037*	243.5*	243.5*	243.5*

*Calculated using the GGA-PBE/Plane-Wave basis sets with ultrasoft pseudopotentials (the energy cutoff was set to 300 eV, the Brillouin zone was sampled at 256 k-points, and an $8 \times 8 \times 8$ k-point mesh was used).

3. Results and discussion

3.1. Thermite reactions of Al/Pd core–shell nanoparticles

As mentioned earlier, after the initial structures were relaxed at six initial temperatures (i.e., 300 K, 400 K, 500 K, 600 K, 700 K and 900 K), the NVE simulations were conducted and the phase changing processes of nanoparticles with varying temperatures were observed. It was expected that, because the reaction between Al and Pd atoms to form the Al–Pd alloy is highly exothermic, when the initial temperature is great enough to overcome the activation energy, a rapid thermite reaction to alloy Al and Pd will occur and the initial core–shell structure will be destroyed quickly. Figure 1, which shows the temperature profiles calculated for processes with different initial temperatures, confirms this expectation.

While the initial temperature of 300 K did not bring about any significant change in the system temperature (similarly for 400 K and 500 K), rapid temperature rises (about 700 K over less than 100 ps) were observed for 600 K, 700 K and 900 K. This shows the thermite reactions occurring above 600 K. Figure 1 reveals three interesting characteristics of the thermite reaction. First, after the thermite reaction occurs and a large amount of heat is generated, different initial temperatures bring about the different adiabatic temperatures in the system. As shown, the final temperatures are 1630 K, 1400 K and 1300 K for the initial temperatures of 900 K, 700 K and 600 K, respectively. This distinction in final system temperatures comes from the different energy contents of the initial nanoparticle. Higher the initial temperature is, the higher total energy the system has. And subsequently the higher temperature will be produced from the thermite reaction. Secondly, the same temperature change (about 700 K) was observed for all three thermite reactions. In order to investigate the energy balance during a thermite reaction, the following process was evaluated under the NVE conditions,

$$\mathrm{A1(core)} + \mathrm{Pd(shell)} \rightarrow \mathrm{A1{-}Pd\,alloy} + \Delta H \qquad (7)$$

Because the above reaction occurs under the adiabatic condition and the system volume does not change, the energy release ΔH is utilized completely to achieve the nanoparticle's structural transformation (i.e., phase change). This change in internal energies ΔH can be measured from the MD simulation. Three values of ΔH (in J/mol Al–Pd alloy) were obtained for different initial temperatures, i.e., 11 897 (for 600 K), 11 665 (for 700 K) and 10 758 (for 900 K).

It is interesting to observe that, the energy release decreases with the increasing initial temperature. For this study, the initial structures consist of separated Al and Pd fcc phases as the core and the shell, respectively. These initial core–shell structures were relaxed at different temperatures (600 K, 700 K and 900 K) and hence possess different kinetic and potential energies. The final alloy phases corresponding to different adiabatic temperatures (1300 K, 1400 K and 1630 K), however, are characterized as the Al–Pd alloy with a space group of Pm3m according to the Al–Pd phase diagram [33]. The structures of these alloys were further studied using the pair correlation function $g(r)$, which is defined as the probability of finding the center of a particle (e.g., the Al atom) for a given distance from the center of a known particle (e.g., the Pd atom). Figure 2 shows the $g(r)$ calculated for these alloyed nanoparticles generated from different initial temperatures. The calculation method shown in literature [34] was used. It shows that, after the simulation period of 300 ps, three alloyed Al/Pd nanoparticles exhibit the nearly identical $g(r)$. In addition, the Al–Pd pairs with an average distance of 2.69 Å were found as the dominant structure for all three nanoparticles. This value agrees very well with the reported inter-atomic distance between an Al atom and the nearest Pd atom in the bulk B2 Al–Pd alloy (2.64 Å) [31]. The similarity in the structures of produced nanoparticles suggests that, although formed through different reaction paths and with varying initial temperatures, the final products of the thermite reaction of the 5 nm Pd coated Al nanoparticles are the solid-phase Al–Pd alloy. This does not conflict with the much higher melting point of Al–Pd alloy 1918 K [33]. Based on this analysis, it can be concluded that the energy release from the thermite reactions

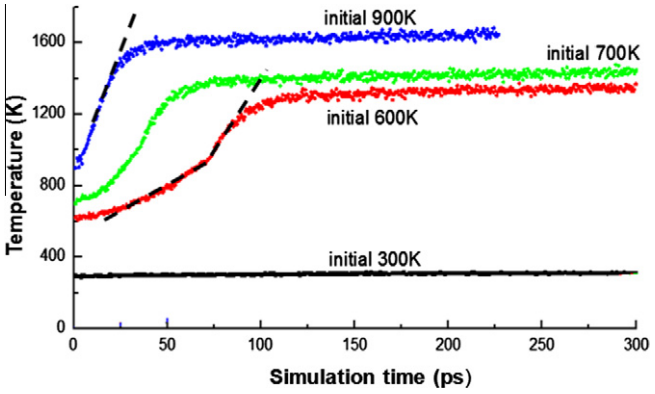

Figure 1. Temperature profiles predicted for Al/Pd core–shell nanoparticles with different initial temperatures. The dash lines show different stages of the reaction.

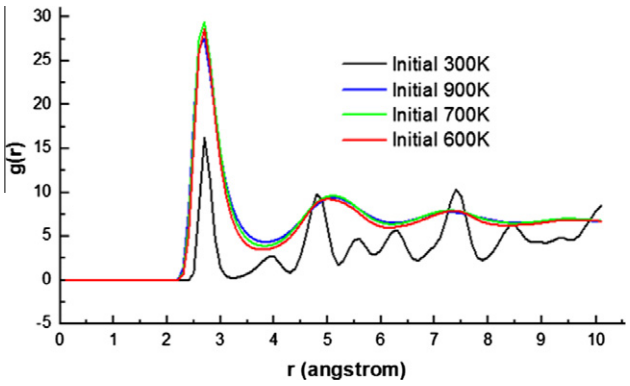

Figure 2. The pair correlation function $g(r)$ calculated for Al–Pd alloy nanoparticles with different initial temperatures.

initiated from different temperatures is mainly determined by the structure of core–shell nanoparticles in the beginning.

Thirdly, Figure 1 shows a higher initial temperature leads to a faster thermite reaction. For example, it takes about 30 ps for alloying the Al–Pd nanoparticle from the initial temperature of 900 K and about 125 ps from the initial temperature of 600 K. If the slopes for these temperature curves in Figure 1 are plot, as shown by dash lines, it is easy to find that, the curve of 600 K exhibits a two-stage process while the one for 900 K contains only one process. Please note that for 900 K, a small temperature increase (about 40 K) occurs at very short reaction time (about 1–2 ps). This implies a structural buffer process through which a different initial structure with a liquid Al core (as discussed later) was obtained. This two-stage mechanism of thermite reactions for lower temperatures such as 600 K and 700 K is important and was studied by investigating the roles of diffusion during the thermite reaction.

3.2. Diffusion and its role in nanothermite reactions

At different temperatures, the Al/Pd core–shell nanoparticles can possibly endure solid-state and liquid (if the Al core melts) diffusion. It was found that for Ni coated Al nanoparticles, the differences in the size-dependent melting temperature can lead to distinguishable energetic characteristics of the nanothermite [17]. In this study, a special attention was paid to understand the effects of solid-state and liquid diffusion processes on the two-stage reaction mechanism shown earlier. Figure 3 shows snapshots of the MD simulation for the initial temperature of 600 K. At 50 ps when the evolving temperature is 740 K (shown in Figure 1), the localized alloying reaction is observed in a zone close to the upper Al–Pd interface where the Pd shell is thin. Note that most of the Al core remains its fcc phase although the temperature is higher than the previously reported melting temperature of 620 K for 4.4 nm pure Al nanoparticles [14]. This appearance of the solid Al core at 740 K (vs. 620 K) can be possibly explained by an increase in the melting point of the Al core due to the repressive Pd shell. The similar behavior was observed in Ni coated Al nanoparticles for which the melting point of the Al core was increased by about 200 K due to the existence of the Ni shell [14]. For this moment of 50 ps when the reaction occurs at its first stage, some Al atoms have diffused at the solid state into the upper Pd shell. The Al–Al and Pd–Pd bonds are replaced by new Al–Pd bonds and the energy release from this process results in the increasing system temperature. At 90 ps (Figure 3c) when the temperature reaches 1150 K, the alloying reaction occurs at a much larger zone and the appearance of Al atoms can be found over the entire Pd surface. Meanwhile some Pd atoms have entered into the Al core which presents a liquid-phase behavior. At this moment, a two-way diffusion phenomenon occurred (i.e., Al diffuses into Pd and Pd diffuses into Al) and intensive alloying between Al and Pd occurs [14]. This results in a faster reaction rate shown at the second stage of the thermite reaction. At 300 ps when the maximum adiabatic temperature is reached, the alloying reaction slows down (since the available Al–Al and Pd–Pd bonds are consumed) and finally the equilibrium structure of Al–Pd alloy is formed.

The diffusion of Al atoms from their initial lattice locations can be further studied by calculating the equivalent volume of the entire Al atom population at a specific reaction time. For this purpose the inter-atomic distance between each pair of Al–Al atoms was accounted and the average diameter for a sphere containing all these Al atoms was derived. Such diameters calculated for Al atoms and Al–Pd atoms are shown in Figure 4. It shows that for each initial temperature, when the volume of the Al core increases with the ongoing reaction time, the volume of the entire Al–Pd nanoparticle does not change. For the 600 K curve, the diameter of Al core increases slowly from the beginning (0 ps), this implies an active solid-state diffusion of Al atoms at this temperature. The slope of the diameter curve keeps constant until above 50 ps, which confirms that the solid-state diffusion dominates during the first stage.

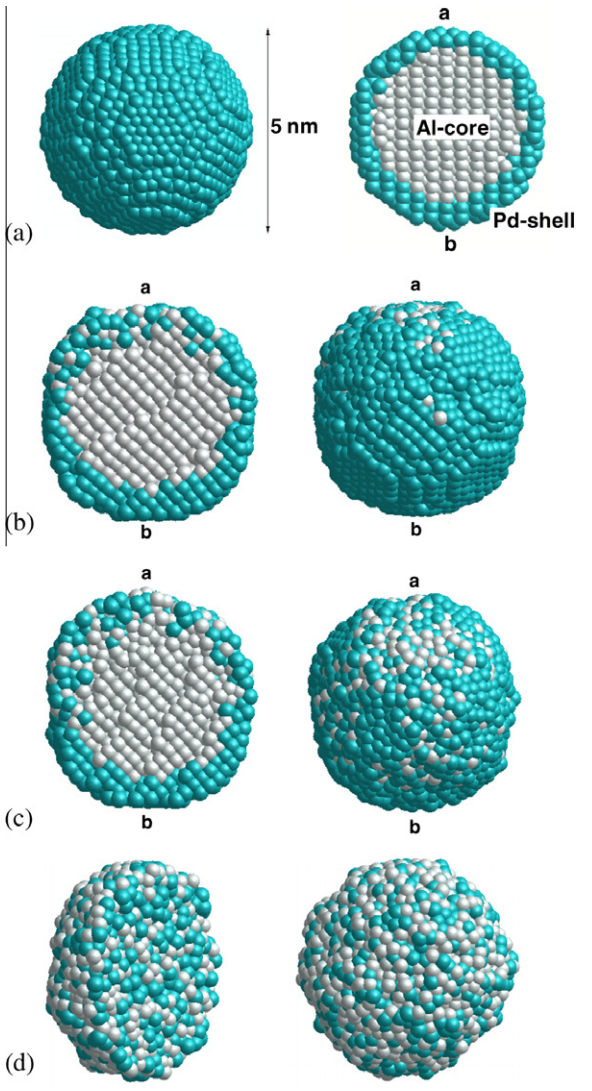

Figure 3. Snapshots of the MD simulation for the initial temperature of 600 K. (a) 0 ps; (b) 50 ps; (c) 90 ps; and (d) 300 ps.

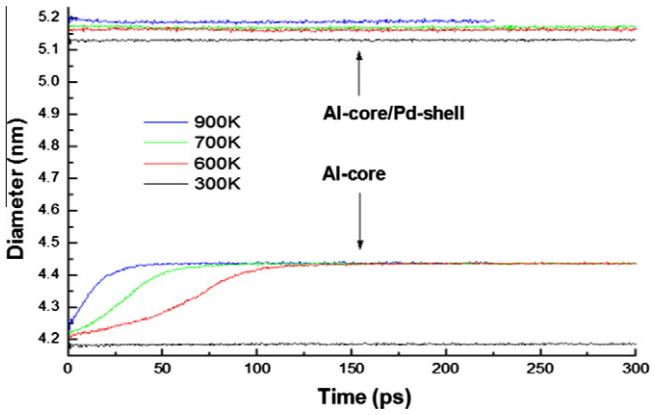

Figure 4. Changes in the volume of the Al core and the Al/Pd core–shell nanoparticles with time for different initial temperatures.

As mentioned earlier, there are defects (away from the fcc structure) existing along the Al–Pd interface in the asymmetrical initial structure. These defects can promote the solid-state diffusion close to the interface.

Figure 4 also shows, the diameters of the initial Al core and Al/Pd core–shell are dependent on the temperature. While the initial diameter of the Al core is 4.19 nm at 300 K, its diameter is 4.23 nm at 900 K. Similarly, the diameters of the Al/Pd core–shell nanoparticles are 5.13 nm and 5.18 nm for 300 K and 900 K, respectively. These differences confirm the different energy contents that initial nanoparticles have. The diffusion pathways of Al and Pd atoms can be further characterized using their average root-mean-square-distances (RMSD) by tracking individual atoms. Given two sets of n points v and w, the RMSD is defined as follows

$$RMSD(v,w) = \sqrt{\frac{1}{n}\sum_{i=1}^{n} \|v_i - w_i\|^2} \quad (8)$$

The RMSD calculated for Al and Pd atoms for each initial temperature are shown in Figure 5. Generally speaking, the mobility of Pd atoms is smaller than Al atoms at the same temperature. This may imply the solid-phase behavior of Pd atoms during the reaction and agrees with a higher melting point of the bulk Pd (1828 K) than the bulk Al (933 K) [33]. It is interesting to investigate the behaviors of Al atoms in both 600 K and 900 K cases. At 600 K, the RMSD of Al and Pd atoms are about equal up to 50 ps. This reflects statistically a negligible alloying process and shows the diffusion of Al atoms is localized (as shown in Figure 3b). The mobility of Al atoms increases dramatically after the reaction time is greater than 50 ps. This is due to the significant phase change close to its melting structure. At 900 K, the mobility of Al atoms is much larger than Pd atoms in the beginning, which implies a melting Al core. This molten Al core brings about a single-stage thermite reaction process without the contribution of the solid-state diffusion of Al atoms.

3.3. Thermal stability at 300 K

Figures 1 and 4 show for the core–shell nanoparticle at the initial temperature of 300 K, there is no significant change in the system temperature and volume. This observation agrees with the $g(r)$ function revealed in Figure 2 and confirms a heterogeneous Al/Pd binary structure across the simulation period (up to 1000 ps). The snapshots of this MD simulation at 300 K are shown in Figure 6. At 300 ps, a few Al atoms are able to rupture the Pd shell and reach the outer surface of the nanoparticle. At 600 ps, more Al atoms diffuse to the outer surface of the nanoparticle. Please note that during this process both the Al core and the Pd shell remain their fcc lattices. This suggests that at 300 K, the solid-state diffusion of Al atoms is quite localized and the energy release from the alloying reaction is insignificant.

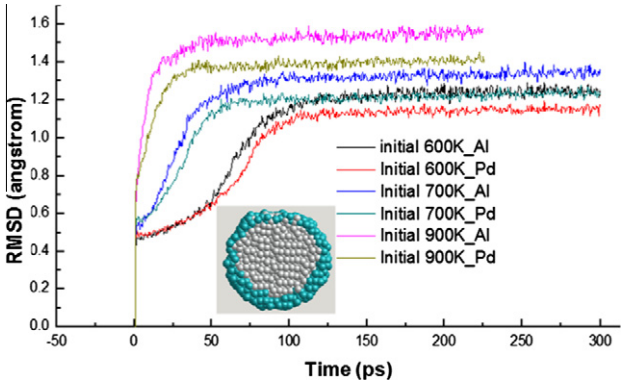

Figure 5. RMSD of the Al and Pd atoms calculated for three processes with different initial temperatures.

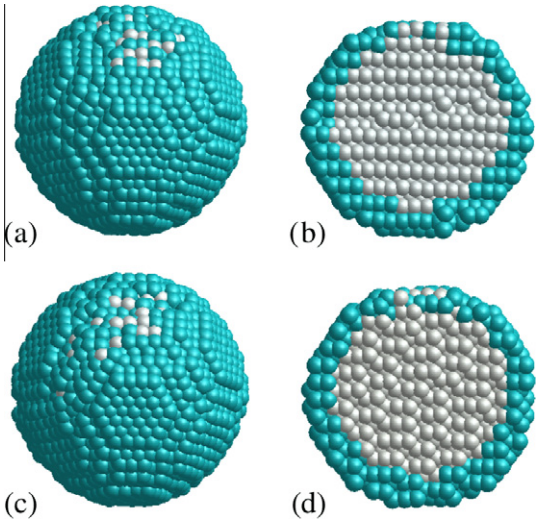

Figure 6. Snapshots of MD simulated structures for the initial temperature of 300 K. (a,b) at 300 ps; (c,d) at 600 ps.

4. Conclusion

The thermal stability and reaction mechanism of the Al/Pd core–shell nanoparticle were studied using a new force field model. The force field parameters for the Al–Pd binary system were found on basis of the reported second moment approximation for tight-binding (TB-SMA) models for pure Al and Pd metals. A localized alloying reaction between the Al core and Pd shell was observed with a much slower rate at lower temperatures such as 300 K. When the initial temperature is higher such as 600 K and 700 K, a two-stage thermite reaction was observed. At the first stage, the reaction rate is determined by the solid-state diffusion of Al atoms in the Pd shell. At the second stage when the particle temperature is greater than the melting point of its Al core, the reaction rate increases dramatically due to alloying between the liquid Al core and the Pd shell. At higher temperatures such as 900 K, the thermite reaction occurs directly between the liquid Al core and the Pd shell. It was observed that different initial temperatures brought about the different final adiabatic temperatures after the thermite reactions occur and the energy release from a thermite reaction varies with its initial temperature. The future work may include investigating the size-dependent properties of the Al/Pd core–shell nanothermite and the effect of the thickness of the Pd-shell on the thermal stability of nanoparticles.

Acknowledgments

This project is supported by NSERC (Natural Sciences and Engineering Research Council of Canada) through an Engage grant.

References

[1] C. Rossi, K. Zhang, D. Esteve, P. Alphonse, P. Tailhades, C. Vahlas, J. Microelectromech. Syst. 16 (2007) 919.
[2] K. Sullivan, M.R. Zachariah, J. Propul. Power 26 (2010) 467.
[3] A. Prakash, A.V. McCormick, M.R. Zachariah, Nano Lett. 5 (2005) 1357.
[4] R. Shende et al., Propellants Explos. Pyrotech. 33 (2008) 122.
[5] J.A. Puszynski, J. Therm. Anal. Calorim. 96 (2009) 677.
[6] K.J. Blobaum, M.E. Reiss, J.M.P. Lawrence, T.P. Weihs, J. Appl. Phys. 94 (2003) 2915.

[7] J.L. Cheng, H.H. Hng, H.Y. Ng, P.C. Soon, Y.W. Lee, J. Phys. Chem. Solids 71 (2010) 90.
[8] K. Zhang, C. Rossi, G.A.A. Rodriguez, C. Tenailleau, P. Alphonse, Appl. Phys. Lett. 91 (2007) 113117.
[9] Z.P. Cheng, F.S. Li, Y. Yang, Y.L. Yang, X.D. Liu, Rare Met. Mater. Eng. 36 (2007) 713.
[10] Z.P. Cheng, Y. Yang, X.D. Liu, Y.L. Yang, F.S. Li, Acta Chim. Sinica 65 (2007) 81.
[11] F. Delogu, Nanotechnology 18 (2007) 505702.
[12] A.V. Evteev, E.V. Levchenko, D.P. Riley, I.V. Belova, G.E. Murch, Philos. Mag. Lett. 89 (2009) 815.
[13] E.V. Levchenko, A.V. Evteev, D.P. Riley, I.V. Belova, G.E. Murch, Comput. Mater. Sci. 47 (2009) 712.
[14] P.X. Song, D.S. Wen, J. Phys. Chem. C 114 (2010) 8688.
[15] S.H. Fischer, M.C. Grubelich, Theoretical Energy Release of Thermites, Intermetallics, and Combustible Metals, Sandia National Laboratories, Albuquerque, NM, 1998.
[16] Z. Kuntova, G. Rossi, R. Ferrando, Phys. Rev. B: Condens. Matter 77 (2008).
[17] B.J. Henz, T. Hawa, M. Zachariah, Mol. Simul. 35 (2009) 804.
[18] A.V. Evteev, E.V. Levchenko, I.V. Belova, G.E. Murch, Phys. Chem. Chem. Phys. 11 (2009) 3233.
[19] E.S. Zijlstra, S.K. Bose, M. Klanjsek, P. Jeglic, J. Dolinsek, Phys. Rev. B: Condens. Matter 72 (2005) 174206.
[20] S.P. Kuruvilla, C.S. Menon, in: Ferromagnetic Shape Memory Alloys, 2008, p. 135.
[21] B. Zhang, X.Z. Li, W. Steurer, J. Schneider, F. Frey, Philos. Mag. Lett. 72 (1995) 239.
[22] U. Koster, P.S. Ho, M. Ron, Thin Solid Films 67 (1980) 35.
[23] K.P. Rodbell, D.B. Knorr, J.D. Mis, J. Electron. Mater. 22 (1993) 597.
[24] M.S. Daw, M.I. Baskes, Phys. Rev. B: Condens. Matter 29 (1984) 6443.
[25] B. Loisel, D. Gorse, V. Pontikis, J. Lapujoulade, Surf. Sci. 221 (1989) 365.
[26] F. Cleri, V. Rosato, Phys. Rev. B: Condens. Matter 48 (1993) 22.
[27] M.A. Karolewski, Radiat. Eff. Defects Solids 153 (2001) 239.
[28] J.L. Shao, C. Yang, X.L. Zhu, X.H. Lu, J. Phys. Chem. C 114 (2010) 2896.
[29] J.D. Gale, A.L. Rohl, Mol. Simul. 29 (2003) 291.
[30] W.M. Haynes, CRC Handbook of Chemistry and Physics, Taylor and Francis Group, LLC, 2011.
[31] P. Eckerlin, H. Kandler, Structure Data of Elements and Intermetallic Phases, Springer-Verlag, Berlin, 1971.
[32] Tables of Physical and Chemical Constants, 16th ed., Kaye & Laby, 1995. Available from: www.kayelaby.npl.co.uk.
[33] H. Okamoto, J. Phase Equilib. 24 (2003) 196.
[34] A. Ben-Naim, R. Mountain, J. Chem. Phys. 128 (2008) 214504.